The architecture of the DNA replication origin recognition complex in *Saccharomyces cerevisiae*

Zhiqiang Chen*†‡, Christian Speck†§¶, Patricia Wendel§, Chunyan Tang*, Bruce Stillman§‖, and Huilin Li*‖**

*Biology Department, Brookhaven National Laboratory, Upton, NY 11973; §Cold Spring Harbor Laboratory, 1 Bungtown Road, Cold Spring Harbor, NY 11742; and **Department of Biochemistry and Cell Biology, Stony Brook University, Stony Brook, NY 11794

The origin recognition complex (ORC) is conserved in all eukaryotes. The six proteins of the *Saccharomyces cerevisiae* ORC that form a stable complex bind to origins of DNA replication and recruit prereplicative complex (pre-RC) proteins, one of which is Cdc6. To further understand the function of ORC we recently determined by single-particle reconstruction of electron micrographs a low-resolution, 3D structure of *S. cerevisiae* ORC and the ORC–Cdc6 complex. In this article, the spatial arrangement of the ORC subunits within the ORC structure is described. In one approach, a maltose binding protein (MBP) was systematically fused to the N or the C termini of the five largest ORC subunits, one subunit at a time, generating 10 MBP-fused ORCs, and the MBP density was localized in the averaged, 2D EM images of the MBP-fused ORC particles. Determining the Orc1–5 structure and comparing it with the native ORC structure localized the Orc6 subunit near Orc2 and Orc3. Finally, subunit–subunit interactions were determined by immunoprecipitation of ORC subunits synthesized *in vitro*. Based on the derived ORC architecture and existing structures of archaeal Orc1–DNA structures, we propose a model for ORC and suggest how ORC interacts with origin DNA and Cdc6. The studies provide a basis for understanding the overall structure of the pre-RC.

electron microscopy | structure | ATPase

In *Saccharomyces cerevisiae* origins of DNA replication contain conserved A, B1, and B2 elements, where the A element and part of B1 define the binding sequence for the origin recognition complex (ORC) (1–3). ORC binds to origin DNA in an ATP-dependent manner and recruits other essential proteins, such as the initiation factors Cdc6, Cdt1, and the presumptive DNA helicase MCM, to the autonomously replicating sequence (ARS) to form a prereplicative complex (pre-RC) before the initiation of DNA replication that occurs in S phase (4–7). ORC consists of six proteins named in the descending order of their relative mass: Orc1 (120 kDa), Orc2 (71 kDa), Orc3 (62 kDa), Orc4 (56 kDa), Orc5 (53 kDa), and Orc6 (50 kDa). The calculated mass of ORC is ≈412 kDa. Only two of the ORC subunits (Orc1 and Orc5) are known to bind ATP (8), although the largest five subunits are predicted to contain an AAA+ fold and a DNA-binding winged helix domain (WHD) within their C-terminal halves (9, 10).

The prokaryotic origin recognition proteins consist of a single polypeptide that can form oligomeric structures (11–17), which raises the question of why in eukaryotes ORC has six subunits and why Cdc6 also contributes to origin recognition (18, 19). Structural studies of the replication initiator proteins have begun to shed light on the mechanism of origin recognition, but how individual initiator proteins cooperate to promote initiation of DNA replication is not clear. The eubacterial DnaA structure suggested that the origin DNA might wrap around a super helical assembly of multiple subunits of this replication initiator (11, 12). In contrast, the recent structures of archaeal Orc1/Cdc6 in complex with DNA implicates a different mechanism in which the initiators wrap around DNA (14, 17). The low-resolution EM structures of ORC from yeast and *Drosophila* are similar in size

and overall architecture, but with appreciable difference in details (9, 10). So far, crystallographic studies of ORC have not been successful, possibly because the multiple-subunit structure is not very rigid in the absence of DNA and a DNA of ~50 base pairs (bp) long might be required to fully stabilize the structure (10, 20, 21). To gain further insight into the low-resolution EM map, we studied the subunit arrangement of ORC by using a structure-based strategy of systematic maltose binding protein (MBP) fusion in combination with 2D image classification and a biochemical strategy of *in vitro* transcription-translation and coimmunoprecipitation to define subunit–subunit interactions. A model for ORC is presented based on these studies.

Results

EM and Single-Molecule Analysis of ORC Particles. Purified ORC and its derivatives either lacking the Orc6 subunit or containing MBP attached to single subunits were visualized by transmission EM after negative staining. ORC appears to be an elongated particle in raw EM images (Fig. 1*A*). The raw particle images were subjected to multivariate statistical analysis and classification. Images within the same classes were averaged to produce the class averages. The structural features in the 2D class averages of ORC match closely with the reprojections of the 3D map that we have derived previously (Fig. 1*A Inset Left* and *Right*, respectively). In the most commonly observed view of ORC, there are seven high-density regions that are labeled from top to bottom with α through η (Fig. 1*B Upper Left*). The 3D structure of ORC has the dimensions of ≈160 × 130 × 100 Å (ref. 10 and Fig. 1*C*). Comparison of the class averages of various ORC preparations enabled location of the MBP tag associated with ORC. The subunit localization result by EM method was further compared with data obtained from biochemical mapping experiments.

Localization of Orc6 in ORC. In the absence of Orc6, Orc1-5 could still form a stable subcomplex (21). This subcomplex provided us an opportunity to localize the Orc6 in the ORC structure by difference map in either 2D class averages or 3D reconstructions. The raw EM images of Orc1-5 were virtually indistinguishable from that of ORC. However, in selected 2D class averages, the density in the region of Orc1-5 between ς and η, as indicated by a red arrow in Fig. 1*B Lower*, was appreciably weaker than that in the same region of ORC. We assigned this region as the
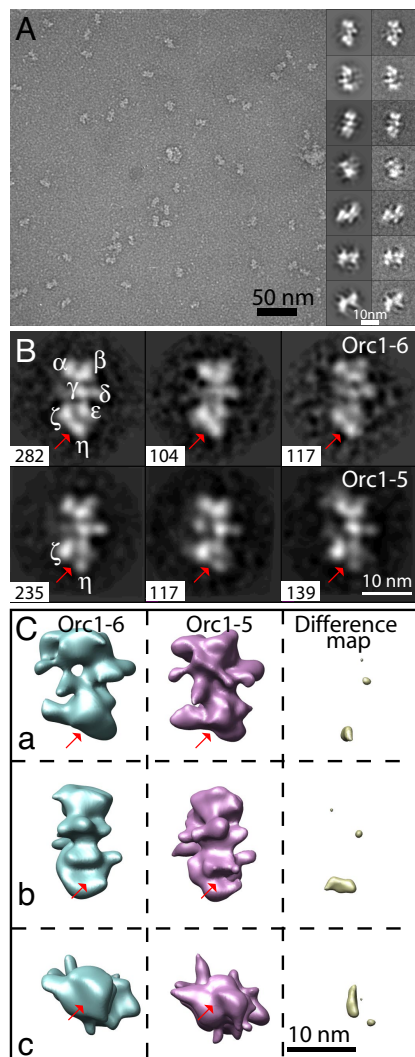
Fig. 1. EM structures of the yeast ORC (Orc1-6) and Orc1-5 subcomplex. (*A*) A raw electron micrograph of the untagged ORC deeply stained by uranyl acetate showing various views. (*Inset*) Seven reprojections of the derived ORC 3D map (*Left*) and the corresponding 2D class averages (*Right*). (*B*) A comparison of three typical side views of ORC (*Upper*) with that of Orc1-5 (*Lower*) reveals the position of Orc6, as indicated by the red arrow. The number in each view refers to the raw particle images used for calculating the reference-free class average. The Greek letters α through η indicate the seven high-density regions in the averaged images. (*C*) Surface-rendered views of the 3D EM maps of ORC (*Left*) and Orc1-5 (*Center*). (*Right*) The difference map at the threshold of 3σ. The largest difference density represents the Orc6 position. *b* and *c* are views rotated 90° from *a* around a vertical and a horizontal axis, respectively.

location of Orc6 in ORC. We further determined the 3D structure of this partial complex. The overall size and structure of Orc1-5 subcomplex was similar to ORC (Fig. 1 *B* and *C*). The 3D difference map confirmed the location assignment of Orc6 (Fig. 1*C Right*). At the display level (3σ), the main difference peak encloses a volume corresponding to ≈32 kDa of protein mass. This mass accounts for 60% of the expected 50-kDa mass of Orc6. We note that the peripheral location of Orc6 is consistent with the knowledge that Orc6 is dispensable in the DNA binding activity of ORC (21–23).

Preparation and Characterization of the MBP-Fused ORCs. Initially, immunolabeling experiments were used to map the subunit organization. ORC was incubated with the Fab fragments (≈50
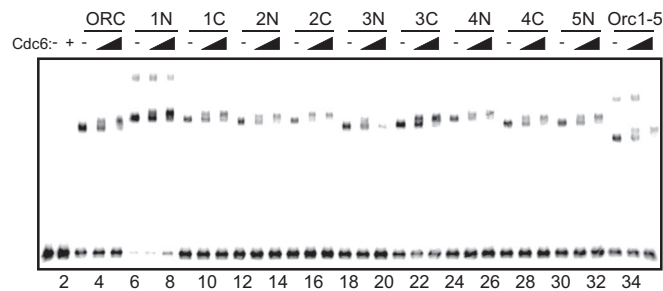

Fig. 2. The MBP-fused ORCs are active in binding to Cdc6 and DNA. Gel-shift assay of ^{32}P-labeled ARS1 DNA with ORC, Cdc6, and MBP-fused ORC complexes or Orc1-5 subcomplex as indicated. The gel-shift assay was performed with 2 nM concentrations of the various ORCs, 0.2 nM of the concentrations labeled ARS1 DNA, and 0.8–2.4 nM of the concentrations Cdc6.

kDa) of four antibodies recognizing Orc1, Orc2, Orc3, and Orc4, respectively, and the Fab–ORC complexes were further purified by gel filtration column chromatography. Although stable Fab–ORC complexes could be seen, no significant densities were observed for the Fab in either the 2D class averages or the 3D reconstructions of the four Fab–ORC complexes (data not shown). The failure was probably caused by the low occupancy of Fab.

To overcome the difficulty in immunolabeling, the *Escherichia coli* MBP (≈38 kDa) was fused to either the N or the C terminus of each of the largest five subunits (Orc1, Orc2, Orc3, Orc4, and Orc5), with a 9-aa linker. Of the 10 constructs prepared, we were able to purify nine MBP-fused ORCs; the one exception was ORC with MBP fused to the C terminus of Orc5 [Orc(1-4,6)–Orc5–MBP]. SDS/PAGE showed that all nine purified MBP-fused ORCs were properly assembled (data not shown). Furthermore, all MBP-fused ORCs, together with the Orc1-5 subcomplex, were able to bind to the ARS1 origin and bind Cdc6 to form an ORC–Cdc6 complex on the origin DNA, as indicated by the Cdc6-induced supershift (Fig. 2). The experiment demonstrated that MBP fusion did not affect the ability of ORCs to interact with DNA or Cdc6. In one case, the MBP–Orc1–ORC complex, DNA binding was significantly enhanced compared with native ORC, suggesting that the N terminus of Orc1 may modulate DNA binding.

Subunit Localization in the MBP-Fused ORCs. The purified ORCs that contained MBP were prepared for EM characterization. We were able to detect MBP in seven of nine ORCs that contained MBP; the MBP in the MBP–Orc1–Orc(2-6) and MBP–Orc2–Orc(1, 3-6) complexes (i.e., MBP fused to the N termini) was not visible, even though we could calculate well defined 2D class averages of these complexes that were essentially the same as that of the native ORC (data not shown). Fig. 3 shows 10 selected reference-free 2D class averages representing the most common view for each of the seven MBP-fused ORCs. Each of these images was an average of a large number of raw particle images, ranging from 45 to 450 particles. Therefore the structural features in these averages are statistically significant. Well defined density, away from the main body of ORC, was present, and these densities in different images of the same fusion ORC were generally clustered to a small area, as shown in illustrations (Fig. 3 *Far Right*). We assigned the extra density to the ≈38-kDa MBP. Thus the location of the observed MBP density reflected the approximate position of the N or C terminus of the corresponding subunit onto which the MBP was fused.

When MBP was observed, its location varied over a small region of the 2D image, most likely because of the ability of the MBP on the N or C termini to occupy alternative, but discrete, positions. The size of the region occupied by MBP most likely

Fig. 3. Detection of MBP in the 2D class averages of the MBP-fused ORC EM images. In each case, the upper row displays 10 class averages from the corresponding MBP-fused ORC and the lower row shows the same images at higher contrast level (contrast = 0.3). In the illustrations (*Far Right*), asterisks mark the observed MBP locations relative to ORC. The number of particles used for calculating each average is indicated. 1C refers to the ORC with MBP fused at the C terminus of Orc1 (ORC–Orc1–MBP). Likewise, the other complexes, 2C, 3N, 3C, 4N, 4C, and 5N also contain MBP at their N or C termini as indicated.

reflected the degree of flexibility of the particular terminus of the ORC subunit to which it was fused. The N and C termini of each of the Orc3 and Orc4 subunits localized to similar sites; however, this did not mean necessarily that they were in the same positions (i.e., the subunit formed a hairpin-like structure), because the images were 2D projections and therefore the N and C termini could be localized in different planes and their position within a 3D space be far apart from each other. MBPs fused to Orc1, Orc4, and Orc5 localized to one side of the ORC, and MBPs fused to Orc2 and Orc3 were located to the opposite side of the ORC, indicating a polarity within the ORC.

ORC Subunit Interactions. To determine the subunit–subunit interactions between the ORC subunits, genes encoding the individual subunits were transcribed and the resulting mRNA was translated in the presence of ^{35}S-methinoine. The labeled proteins were immunoprecipitated either alone or in various combinations (Fig. 4). Orc2 and Orc3 interacted with each other in reciprocal immunoprecipitations (Ips) (Fig. 4 *C* and *D*, lanes 4). Orc4 bound to Orc5 (Fig. 4*A*, lane 16) but not to other individual ORC subunits (Fig. 4*A*, lanes 13–15 and 17). The Orc4/5 complex was able to interact with the Orc2/3 complex (Fig. 4*A*, lane 21, long exposure) and separately with Orc1 (Fig.

4*A*, lane 22, long exposure), and with Orc2/3 and Orc1 to form the Orc1-5 complex (Fig. 4*A*, lane 26). Consistent with these results, the Orc1 antibodies were able to coprecipitate the Orc4/5 complex in the presence of Orc1 (Fig. 4*B*, lanes 9–11). Orc1 did not bind to the individual Orc4 or Orc5 subunits because the bands present in Fig. 4*B*, lanes 4 and 5 were present in beads alone (data not shown). For the same reason we could not test whether Orc1 bound Orc2 or Orc3, but the Orc2/3 complex did not bind to Orc1 (Fig. 4*B*, lane 6). Results for Orc6 binding in these experiments were not consistent or were complicated by Orc6 interacting with the beads in the absence of antibody; and as a consequence, we did not interpret Orc6 interactions.

Discussion

MBP Fusion Combined with 2D Image Classification Is an Effective Approach for Mapping Needs in Molecular EM. Domain or subunit mapping is essential in EM structural studies because of the limited resolution. Antibody labeling or functionalized heavy metal cluster labeling is often used (24, 25). The main difficulty in using these noncovalent labels is low label occupancy, which is further compounded by the flexible nature of the labels. To overcome this difficulty, the use of proteins with encoded molecular tags for EM contrasting was reported (26). The fusion
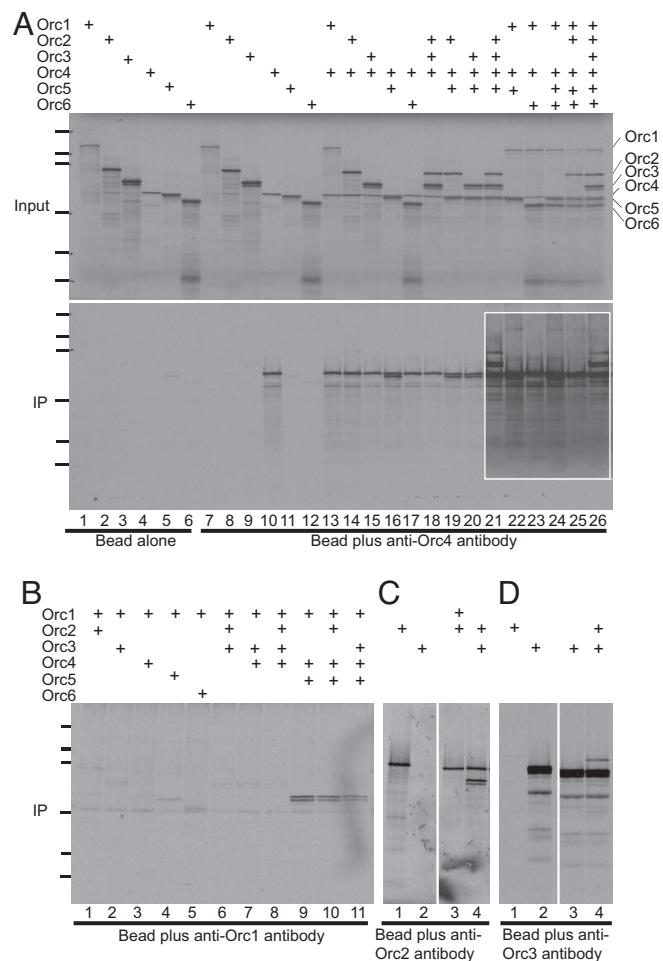
Fig. 4. *In vitro* subunit interaction. (*A Upper*) Genes encoding the individual ORC subunits, cloned into the transcription/translation vector (pCite-2a+), were transcribed and the resulting mRNA was translated individually and in various combinations, 5% of which was run on an SDS/PAGE gel as Input. The remainder of the translation mix was then immunoprecipitated with 20 μl Gamma Bind G Sepharose and washed three times and 50% of the IP mix was loaded onto SDS/PAGE gels. (*A Lower* and *B–D*) The IP of anti-Orc4 (*A Lower*), anti-Orc1 (*B*), anti-Orc2 (*C*), and anti-Orc3 (*D*) antibodies are shown. (*A Lower Inset*) A longer exposure of the gel, which was inserted over the top of the lighter image to observed Orc1 protein. The Orc6 subunit was not observed reliably in the IP lanes and hence we did not assign partners for this subunit.

Fig. 5. The architecture of the yeast ORC. (*A*) A summary of ORC subunit interactions derived from the *in vitro* translation and IP experiments. The Orc6 subunit was not included in the analysis. (*B*) A summary of subunit mapping results. The approximate MBP position represents the location of the corresponding N or C terminus of the subunit onto which the MBP was fused. For an example, 1C refers to the average MBP position found in Orc(2-6)–Orc1–0MBP. (*C*) A proposed model for ORC interaction with Cdc6 and origin DNA. See *Discussion* for details.

protein approach eliminates the occupancy problem and was used previously in the context of 3D difference mapping (27). We found that the flexible fusion protein could be separated efficiently into different 2D classes according to its positions by reference-free 2D image classification. We demonstrated with numerous MBP-fused ORCs that this approach is effective and straightforward. We suggest that the approach of MBP fusion combined with 2D image classification be added to the existing toolkit for locating domains or subunits in large molecular complexes.

Flexible Domains in ORC. Our failure to detect MBP in MBP–Orc1–Orc(2-6) and MBP–Orc2–Orc(1, 3-6) might be caused by the flexibility of the N-terminal domains of Orc1 and Orc2. Conceivably, a flexible MBP fused onto yet another flexible domain would cause the MBP tag to move in too large a range to be visible in averaged images. Similarly, the smaller than expected difference density for Orc6 (Fig. 1*C*) is likely caused by the partial flexibility of the subunit. Indeed, the N termini of
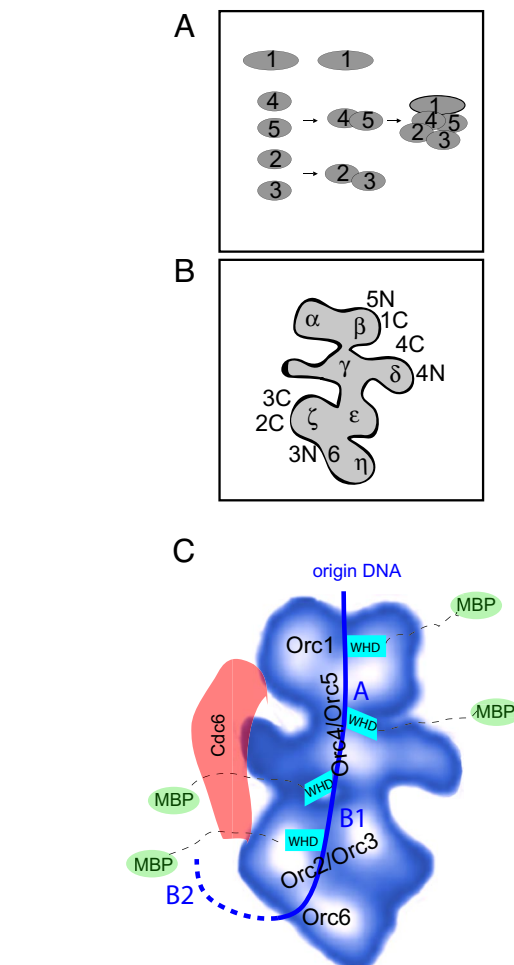
Orc1, Orc2, and Orc6 are most sensitive to proteases, as analyzed by limited proteolysis with ArgC, GluC, thermolysin, and chymotrypsin (data not shown), and these three subunits are the most sensitive to proteases when ORC interacts with Cdc6 and DNA (18). Secondary structure predictions also indicate that the N termini of Orc1, Orc2, and Orc6 are enriched with flexible loop regions (data not shown). The N terminus of Orc1 is involved in interaction with Sir1 (28–30) and Cdc6 (31). These interactions might require a certain degree of flexibility to achieve its function in silencing. Based on these considerations, we suggest that the proposed structure of ORC derived from the native complex does not have all regions of the protein visible (Fig. 5 *B* and *C*).

ORC Architecture. Fig. 5 *A* and *B* summarizes our subunit interaction and the MBP mapping results, respectively. It is clear from these studies that Orc1, Orc4, and Orc5 occupy the upper half, and Orc2, Orc3, and Orc6 occupy the lower half of the structure. The two independent experimental approaches yielded consistent results regarding the relative proximity of subunits to each other. The derived ORC architecture is also in agreement with earlier protein–DNA cross-linking experiments and recent yeast

two-hybrid experiments that suggest or demonstrate a direct contact between Orc2p and Orc3p and between Orc4p and Orc5p (21, 23, 32). It is significant to note that termini of each of the five largest subunits of ORC are clustered to either the upper right area or the lower left area of ORC within the ORC structure (Fig. 5C). The C-terminal part of Orc1-5 contains the proposed DNA-binding winged helix domain (WHD), and N terminal to the WHD is a proposed domain belonging to the class of AAA+ proteins (9, 10). A common feature of oligomeric AAA+ complexes is the location of ATP binding sites at the interface of two different subunits. The interface between subunits frequently contains an arginine finger in one subunit that interacts with the ATP bound by the adjacent subunit. It has been shown that an arginine finger in Orc4 is required to stimulate the ATPase within Orc1 (33). This result indicates that Orc1 and Orc4 interact directly and are thus located adjacent to each other, a result consistent with our proposed structure (Fig. 5C). For human ORC it has been shown that Orc2 and Orc3 form a complex with Orc5 (34–37), indicating that an Orc1–Orc4–Orc5 complex interacts with Orc2–Orc3 via Orc5, and that the Orc2-5 complex binds Orc1, suggesting an order in the complex of Orc1,4,5,2/3. This arrangement is also consistent with a low-resolution EM structure of ORC from *Drosophila* where Orc5 was localized with the help of an antibody in the center of the elongated complex (9). The relative order of Orc2/3 in our proposed structure is not possible to assign based on existing data, and we cannot conclude this order with certainty. However, recent yeast two-hybrid data show an interaction between Orc2 and Orc5 (32), suggesting that hints that Orc3 might represent the one end of the ORC if the AAA+ subunits are arranged in pseudolinear arrangement in the structure.

A Model for Interaction Between ORC, Cdc6, and Origin DNA. The DNaseI footprint analysis suggests a protection of 48 bp of *ARS1* origin DNA by the yeast ORC in the presence of ATP (19, 20). The dimension of our EM structure of ORC is large enough to accommodate five AAA+ domains with WHD, and the 16-nm length is appropriate for covering the 48-bp dsDNA. To estimate the actual DNA contact sites, however, 3 to 5 bp from the ends of the footprint should be subtracted, because DNase1 cannot access the actual DNA binding site due to steric hindrance. Thus, the protein–DNA contacts would likely cover ≈38–44 bp of DNA. The archaeal Orc1 binds to DNA with two claws, one from a WHD and the other from the initiator-specific motif (ISM) in the α/β subdomain of the AAA+ domain (14, 17). In the protein–DNA structure, the WHD binding sites of Orc1–1 and Orc1–3 are 9 bp apart, but at the secondary ISM DNA binding sites these two Orc1 subunits are only 3 bp apart. It is uncertain how a hypothetical third ORC subunit would bind to DNA if the archaeal Orc1–DNA structure was extended by one subunit. Because the WHD is the major DNA binding element, we assume that the WHD defines the spacing between the neighboring subunits. If this assumption were incorporated into a model for the multisubunit eukaryotic ORC, it would result in four adjacent WHD-containing origin-binding subunits in ORC [$3 \times 9 + 15 = 42$ bp, where the 15 bp is the actual DNA-contacting length of each subunit, as estimated from the Orc1–DNA structure (14, 17)]. ORC is predicted to contain five WHD-containing subunits, and we suggest that the fifth WHD in ORC and the Cdc6 WHD might bind DNA when ORC forms a complex with Cdc6, thereby greatly extending the interaction with DNA to ≈80 bp (10).

In the archaeal Orc1–DNA structure, Orc1-1 and Orc1-3 are staggered ≈60° around the DNA axis (14, 17). If this mode of interaction is conserved in the eukaryotic ORC, we suggest a model for ORC in which the origin DNA runs along its length (Fig. 5C). In this model, the above-estimated four major DNA-binding WHDs are ≈60° apart along the DNA axis, resulting in

the first two C-terminal WHD (0° and 60°, respectively) on one side and at one end, with the remaining two C-terminal WHD (120° and 180°, respectively) on the opposite side and at the other end of the proposed structure. This arrangement agrees with the observed clustering of C-terminally fused MBP to the lower left and upper right sides of the ORC structure.

A DNA cross-linking study with ORC and DNA demonstrated that Orc1 and Orc4 bind near the A element and Orc2 and Orc3 bind near the B1 element of the *ARS1* origin (21). These data suggest that the A element binds to the upper half of ORC where Orc1 and Orc4 are located and B1 binds to the lower half where Orc2 and Orc3 reside. Such a DNA orientation would point Orc6, located at the bottom of ORC, toward B2 (Fig. 5C), in agreement with the knowledge that Orc6 interacts with DNA near B2. We previously showed that Cdc6 binds to the left side of ORC and Cdc6 caused a profound lengthening of the DNA contact (10). We speculate that B2 might bend back onto ORC in the presence of Cdc6, which also contains a WHD near its C terminus (Fig. 5C). It was shown that the putative replicative helicase MCM loads at the B2 region and that Cdt1, the MCM loading protein, interacts with Orc6 (22, 38, 39).

To summarize, our current understanding of ORC is that the primary recognition is at the *ARS1* A element, with a secondary interaction with the B1 element. This bipartite recognition determines, in part, the origin specificity of ORC and points the non-AAA+ domains in Orc6 and Orc2 toward the *ARS1* B2 element. Cdc6 interaction with ORC extends the DNA interaction toward the B2 element where Cdt1 cooperates to load the MCM proteins. The overall ring-shaped structure of the ORC–Cdc6 complex may facilitate interactions with the hexameric, ring-shaped MCM proteins.

Materials and Methods

Preparation of the MBP-Fused ORCs. To generate ORCs with MBP at its C or N terminus, the MBP coding region was amplified along with a 9-aa linker (AAAAAIDTT) that was fused on either the C or N terminus of each ORC subunit. This modified ORC subunit along with the remaining five nontagged subunits were expressed from recombinant baculovirus vectors in insect cells as described (21). The proteins were purified as described (10).

Gel-Shift Assay. The gel-shift assay was performed as described (10) using 0.2 nM *ARS1* DNA, 2 nM ORC, ORC–MBP fusion complexes, or Orc1-5, and 0.8 or 2.4 nM Cdc6.

ORC Subunit Interactions. Genes encoding *S. cerevisiae* ORC subunits were cloned individually by PCR primer extension and ligated into pCite-2a(+)(Novagen/EMD) at the SacI/XhoI sites. Transcription/translation was carried out with the TNT T7 Coupled Reticulocyte Lysate System, (Promega) using the standard reaction mix and 1 μg of DNA per sample. mAbs [Orc1 (SB13), Orc2 (SB67), Orc3 (SB3), Orc4 (SB6), Orc5 (SB5) and Orc6 (SB49)] were ≈10 mg/ml by protein gel analysis and were used at 2.5 mg per IP reaction. Translation products were diluted 1:5 in buffer [20 mM Hepes-KOH (pH 7.0), 75 mM NaCl, 0.02% Nonidet P-40, 5 mM MgAc, 5 mM β-mercaptoethanol, 1 mM ATP (pH 7.0), 10% glycerol and Complete-EDTA Free Protease Inhibitor tablets (Roche)], combined with clarified mAbs and immunoprecipitated by using Gamma Bind G Sepharose (GE Healthcare), 1 h at 4°C. Proteins (5% input and 50% IP) were visualized after electrophoresis through 10% acrylamide/0.3%Bis SDS/PAGE gels, dried, and exposed to imaging film.

EM. The concentrations of ORC and its derivatives were adjusted to ≈0.1 mg/ml in buffer containing 50 mM Hepes-KOH (pH 7.6), 100 mM potassium glutamate, 5 mM MgCl$_2$, 1 mM EGTA, and 1 mM ATPγS, and the diluted samples were incubated on ice for 15 min. A 6.0-μl drop of sample solution was applied to a glow-discharged 300-mesh copper grid covered with a thin layer of carbon film, and after a brief incubation of 30–60 s, the excess sample solution was blotted with a small piece of filter paper. The grid was then stained in a deep stain procedure by three consecutive 5-μl drops of 2.0% uranyl acetate aqueous solution. Each drop was left on grid for 15–20 s at room temperature before blotting. After blotting the last stain drop, the grid was quickly dried by a stream of argon to prevent crystallization of the stain salt. Micrographs of negatively stained specimens were recorded at a magnifica-

tion of ×50,000 in a JEOL JEM-1200EX transmission EM, operated at an acceleration voltage of 120 kV. All images were recorded on Kodak SO-163 film by using the minimum-dose procedure at the defocus ranging from −1.2 to −1.5 μm. The films were developed for 12 min in a full-strength Kodak D-19 developer at 20°C. Selected micrographs were digitized with a Nikon Super-cool Scan 8000ED using a step size of 12.7 μm.

2D Image Classification and 3D Image Reconstruction. We used SPIDER (40), EMAN (41), and IMAGIC-V (42) programs for image processing. The number of raw particles in each data set was 22,238 (1N), 14,197 (1C), 16,780 (2N), 6,824 (2C), 10,762 (3N), 11,419 (3C), 25,578 (4N), 16,521 (4C), 12,178 (5N), and 8,935 (Orc1-5). The parameters of contrast transfer function for each micrograph were calculated, and these parameters were used for phase flipping. Raw particle images were band-pass-filtered to exclude the very low- and high-frequency noise, normalized, centered, and then subjected to multivariate statistical analysis (MSA) and classification. Several well centered class averages were selected as references to realign all of the raw particle images. The recentered particle images were reclassified. Multireference alignment and classification were carried out for several iterations by using well defined and properly centered class averages from the previous iteration as references until stable class averages were obtained. In a second approach, the MSA and classification were simply carried out by ''2drefine'' in EMAN, (which incorporates the iterative centering, multireference alignment and classification in a single batch script), with an initial class number of 100–150, depending on the data set. The two approaches yielded comparable class averages. The 3D map of the Orc1-5 subcomplex was obtained by refinement in EMAN by using a low-pass-filtered ORC 3D map (30 Å) as the starting model (Speck 2005 NSMB). The 3D difference map was calculated by subtracting the Orc1-5 3D map from the ORC 3D map, after proper scaling. The 3D maps were rendered into surface views with Chimera (43).

1. Marahrens Y, Stillman B (1992) A yeast chromosomal origin of DNA replication defined by multiple functional elements. *Science* 255:817–823.
2. Rao H, Stillman B (1995) The origin recognition complex interacts with a bipartite DNA binding site within yeast replicators. *Proc Natl Acad Sci USA* 92:2224–2228.
3. Rowley A, Cocker JH, Harwood J, Diffley JF (1995) Initiation complex assembly at budding yeast replication origins begins with the recognition of a bipartite sequence by limiting amounts of the initiator, ORC. *EMBO J* 14:2631–2641.
4. Bell SP, Dutta A (2002) DNA replication in eukaryotic cells. *Annu Rev Biochem* 71:333–374.
5. Diffley JF (2004) Regulation of early events in chromosome replication. *Curr Biol* 14:R778—R786.
6. Mendez J, Stillman B (2003) Perpetuating the double helix: Molecular machines at eukaryotic DNA replication origins. *BioEssays* 25:1158–1167.
7. Sclafani RA, Holzen TM (2007) Cell cycle regulation of DNA replication. *Annu Rev Genet* 41:237–280.
8. Klemm RD, Austin RJ, Bell SP (1997) Coordinate binding of ATP and origin DNA regulates the ATPase activity of the origin recognition complex. *Cell* 88:493–502.
9. Clarey MG, *et al.* (2006) Nucleotide-dependent conformational changes in the DnaA-like core of the origin recognition complex. *Nat Struct Mol Biol* 13:684–690.
10. Speck C, Chen Z, Li H, Stillman B (2005) ATPase-dependent cooperative binding of ORC and Cdc6 to origin DNA. *Nat Struct Mol Biol* 12:965–971.
11. Erzberger JP, Mott ML, Berger JM (2006) Structural basis for ATP-dependent DnaA assembly and replication-origin remodeling. *Nat Struct Mol Biol* 13:676–683.
12. Mott ML, Berger JM (2007) DNA replication initiation: Mechanisms and regulation in bacteria. *Nat Rev Microbiol* 5:343–354.
13. Barry ER, Bell SD (2006) DNA replication in the archaea. *Microbiol Mol Biol Rev* 70:876–887.
14. Dueber EL, Corn JE, Bell SD, Berger JM (2007) Replication origin recognition and deformation by a heterodimeric archaeal Orc1 complex. *Science* 317:1210–1213.
15. Singleton MR, *et al.* (2004) Conformational changes induced by nucleotide binding in Cdc6/ORC from *Aeropyrum pernix*. *J Mol Biol* 343:547–557.
16. De Felice M, *et al.* (2004) Modular organization of a Cdc6-like protein from the crenarchaeon *Sulfolobus solfataricus*. *Biochem J* 381:645–653.
17. Gaudier M, Schuwirth BS, Westcott SL, Wigley DB (2007) Structural basis of DNA replication origin recognition by an ORC protein. *Science* 317:1213–1216.
18. Mizushima T, Takahashi N, Stillman B (2000) Cdc6p modulates the structure and DNA binding activity of the origin recognition complex *in vitro*. *Genes Dev* 14:1631–1641.
19. Speck C, Stillman B (2007) Cdc6 ATPase activity regulates ORC × Cdc6 stability and the selection of specific DNA sequences as origins of DNA replication. *J Biol Chem* 282:11705–11714.
20. Bell SP, Stillman B (1992) ATP-dependent recognition of eukaryotic origins of DNA replication by a multiprotein complex. *Nature* 357:128–134.
21. Lee DG, Bell SP (1997) Architecture of the yeast origin recognition complex bound to origins of DNA replication. *Mol Cell Biol* 17:7159–7168.
22. Chen S, de Vries MA, Bell SP (2007) Orc6 is required for dynamic recruitment of Cdt1 during repeated Mcm2 7 loading. *Genes Dev* 21:2897–2907.
23. Chastain PD, 2nd, Bowers JL, Lee DG, Bell SP, Griffith JD (2004) Mapping subunit location on the *Saccharomyces cerevisiae* origin recognition complex free and bound to DNA using a novel nanoscale biopointer. *J Biol Chem* 279:36354–36362.
24. Boisset N, *et al.* (1988) Intramolecular localization of epitopes within an oligomeric protein by immunoelectron microscopy and image processing. *Proteins* 3:161–183.
25. Hainfeld JF (1987) A small gold-conjugated antibody label: Improved resolution for electron microscopy. *Science* 236:450–453.
26. Mercogliano CP, DeRosier DJ (2006) Gold nanocluster formation using metallothionein: Mass spectrometry and electron microscopy. *J Mol Biol* 355:211–223.
27. Liu Z, *et al.* (2001) Three-dimensional reconstruction of the recombinant type 3 ryanodine receptor and localization of its amino terminus. *Proc Natl Acad Sci USA* 98:6104–6109.
28. Hou Z, Bernstein DA, Fox CA, Keck JL (2005) Structural basis of the Sir1-origin recognition complex interaction in transcriptional silencing. *Proc Natl Acad Sci USA* 102:8489–8494.
29. Hsu HC, Stillman B, Xu RM (2005) Structural basis for origin recognition complex 1 protein-silence information regulator 1 protein interaction in epigenetic silencing. *Proc Natl Acad Sci USA* 102:8519–8524.
30. Triolo T, Sternglanz R (1996) Role of interactions between the origin recognition complex and SIR1 in transcriptional silencing. *Nature* 381:251–253.
31. Wang B, *et al.* (1999) The essential role of *Saccharomyces cerevisiae* CDC6 nucleotide-binding site in cell growth, DNA synthesis, and Orc1 association. *J Biol Chem* 274:8291–8298.
32. Matsuda K, *et al.* (2007) Yeast two-hybrid analysis of the origin recognition complex of *Saccharomyces cerevisiae*: Interaction between subunits and identification of binding proteins. *FEMS Yeast Res* 7:1263–1269.
33. Bowers JL, Randell JC, Chen S, Bell SP (2004) ATP hydrolysis by ORC catalyzes reiterative Mcm2–7 assembly at a defined origin of replication. *Mol Cell* 16:967–978.
34. Dhar SK, Delmolino L, Dutta A (2001) Architecture of the human origin recognition complex. *J Biol Chem* 276:29067–29071.
35. Ranjan A, Gossen M (2006) A structural role for ATP in the formation and stability of the human origin recognition complex. *Proc Natl Acad Sci USA* 103:4864–4869.
36. Siddiqui K, Stillman B (2007) ATP-dependent assembly of the human origin recognition complex. *J Biol Chem* 282:32370–32383.
37. Vashee S, Simancek P, Challberg MD, Kelly TJ (2001) Assembly of the human origin recognition complex. *J Biol Chem* 276:26666–26673.
38. Wilmes GM, Bell SP (2002) The B2 element of the *Saccharomyces cerevisiae* ARS1 origin of replication requires specific sequences to facilitate pre-RC formation. *Proc Natl Acad Sci USA* 99:101–106.
39. Zou L, Stillman B (2000) Assembly of a complex containing Cdc45p, replication protein A, and Mcm2p at replication origins controlled by S-phase cyclin-dependent kinases and Cdc7p-Dbf4p kinase. *Mol Cell Biol* 20:3086–3096.
40. Frank J, *et al.* (1996) SPIDER and WEB: processing and visualization of images in 3D electron microscopy and related fields. *J Struct Biol* 116:190–199.
41. Ludtke SJ, Baldwin PR, Chiu W (1999) EMAN: Semiautomated software for high-resolution single-particle reconstructions. *J Struct Biol* 128:82–97.
42. van Heel M, Harauz G, Orlova EV, Schmidt R, Schatz M (1996) A new generation of the IMAGIC image processing system. *J Struct Biol* 116:17–24.
43. Pettersen EF, *et al.* (2004) UCSF Chimera: A visualization system for exploratory research and analysis. *J Comput Chem* 25:1605–1612.

BIOCHEMISTRY

Chen *et al.*